

Depletion of electrons in a multiple substorm event on November 15th, 2001

C. R. Bryant, J. S. Murphree, E. Donovan, and S. B. Mende

Abstract:

Using the IMAGE FUV instrumentation it is possible to determine the power of auroral events. Proton power can be calculated using the SI12 instrument and the power of the LBH spectrum can be calculated using the WIC camera. The resulting power spectrums can be compared, examining the relationship of the precipitating particles. Data will be presented from a multiple substorm event from November 15, 2001.

The multiple substorm event consists of two events that have no apparent IMF trigger during a strong southward IMF (-10 nT). These events are then followed by two substorm events that have external triggers (that being northward turnings). The peaks of the events starting at 1738 UT and 1815 UT have ratios of the SI-12/LBH power of roughly 45%, indicating that the aurora is primarily due to precipitating electrons. The breakup at 1900 UT has a peak of SI-12/LBH power of 170%. Clearly the protons make up much more of the particle precipitation into the auroral oval as the WIC images show weak intensities likely related to secondary electrons from the proton precipitation. The recovery phase after this final substorm is quick for the LBH power but the proton power shows that the decay is longer, perhaps even with another event occurring at 2140 UT with only a proton power signature.

Loss cone for the electrons means they are favoured to precipitate into the oval but are depleted in the later substorm and protons make up the majority of the precipitating particles. Particle measurements will be used in conjunction with images from IMAGE FUV instruments to help determine the relationship between the protons and electrons in this multiple substorm event scenario.

Key words: substorms, IMAGE FUV, multiple events.

1. Introduction

November 15th, 2001 provides an interesting example of a multiple substorm event. In this example, observations reveal an extended growth phase with a strongly southward IMF, a non-IMF triggered pseudo-breakup and breakup, and two breakups triggered by northward turnings. The recovery phase of each part of the event is interesting as many of the features remain when the next breakup occurs in another portion of the oval.

The far ultraviolet instruments on board the IMAGE satellite are the primary vehicle for the selection of the dataset used in this paper. In particular, the wideband imaging camera (WIC) and a spectral imager (SI-12) are used. The WIC instrument operates in the Lyman-Birge-Hopfield (LBH) band from 140 - 190 nm where the prominent excitation mechanism is electron impact excitation for the LBH band [7]. Due to O₂ absorption in part of the LBH band there are significant losses as well as dayglow associated with solar radiation on the dayside. As well, there is also contamination from precipitating protons which are efficient at creating secondary electrons contaminating the pure electron signal [9, 3]

The SI-12 imager measures Doppler shifted Lyman- α emission at 121.567 nm produced by energetic protons cascading into the atmosphere. Geocoronal emissions due to solar radi-

ation at 121.6 nm is a concern but is filtered out to produce only photons associated with proton aurora. Due to limitations of the instrument, however, only protons with energies of at least several keV will be detected [8].

Other than IMAGE FUV, ACE solar wind and interplanetary magnetic field measurements are also used in describing the events. The ACE data is Weimer-mapped from the ACE location near the L1 point back to the bow shock at 12 MLT. This means that the displayed ACE data is much closer to the time that the magnetosphere would actually react to the solar wind and magnetic field.

Using the MLT images for the WIC and SI-12 cameras, it is possible to estimate the power [2]. In this paper, the auroral substorm power is estimated by contouring the hemisphere with a minimum value that was calculated from multiple images of quiet time. Once this minimum level is defined, the contour is run in order to calculate the area [1] of the auroral intensity above the quiet level. Therefore a power level of zero represents a quiet oval.

The auroral substorm power, like other indices such as AE [10], can be used to determine onset/expansion and beginning of the recovery phase. The power dramatically increases at onset. At the beginning of the recovery phase, the power reaches a maximum. As the recovery phase continues, the power continues to decrease until it reaches zero which would indicate the end of the recovery phase.

2. Observations

Looking at the two hours prior to the event, Weimer-propagated ACE data in the figure 1 reveals that there would likely be two

Received 25 May 2006.

C. R. Bryant, J. S. Murphree, and E. Donovan. Institute for Space Research, University of Calgary, Calgary, AB, CAN
S. B. Mende. Space Science Laboratory, University of California, Berkeley, CA, USA

substorms due to northward turnings following the strongly southward B_z period. The growth phase for these two substorms appears to start with a sudden drop of B_z from 5 nT to -7 nT at 1642 UT. It is followed 5 minutes later by a downward shift of B_y . B_z is strongly southward for about 90 minutes before the first northward turning and the first of two externally triggered events.

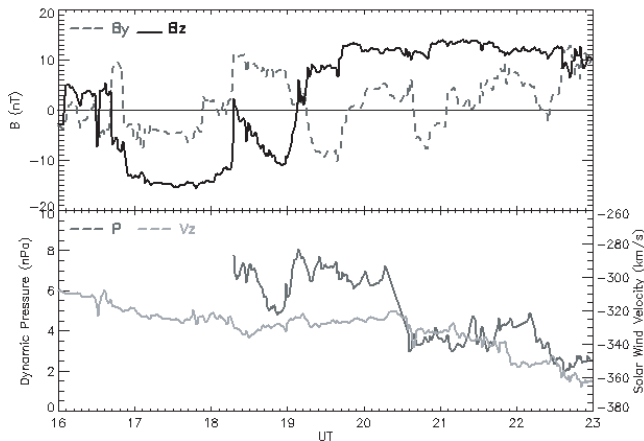


Fig. 1. Weimer-mapped ACE data from 16-23 UT on November 15, 2001. The top panel shows the B_z and B_y components of the solar wind while the lower panel shows the dynamic pressure and the V_x component of the solar wind. (Data is courtesy of Dr. J. Weygand at IGPP, UCLA.)

The growth phase is also evident in figure 2. One expects the poleward edge of the auroral oval to move equatorward during the loading process as the tail is stretched out. Examining the four keograms, the WIC and SI-12 keograms at 3.0 MLT clearly show equatorward movement of the poleward boundary until the first breakup at 1737 UT. The keograms at 23.0 MLT also show equatorward movement but show a potential pseudo-breakup near 1636 UT and then show expansion both equatorward and poleward at the first clear pseudo-breakup at 1720 UT.

The substorms externally triggered by the two separate northward turnings are at 1815 UT and 1900 UT. The first northward turning, from -13 nT to 2 nT, occurs simultaneously with a duskward shift in B_y as seen in figure 1. In figure 2 it is clearly seen that there are increases in intensity at 1815 in both local times. The 1900 UT substorm is not nearly as clear in the MLT images although there is an increase in the intensity of the SI-12 keograms. In figure 3, there is a very clear rise in power starting at 1815 UT. A similar increase is also seen in the SI-12 power. Figure 4 ratio of SI-12 to WIC power is less than 100% during this substorm.

After spiking at 2 nT at 1815 UT, B_z begins to fall off to -10 nT loading energy into the system again over the next 45 minutes. The second northward turning beginning at 1900 UT has a gradual rise in B_z from -10 nT to 8 nT that lasts nearly 8 minutes. At the same time, B_y again moves downward. In this case, the keograms in figure 2 barely show any intensity increase and it appears later than 1900 UT. Most of the intensity increase is also in the post-midnight sector. Similarly, figure 3 shows the SI-12 power increasing at 1900 UT while the

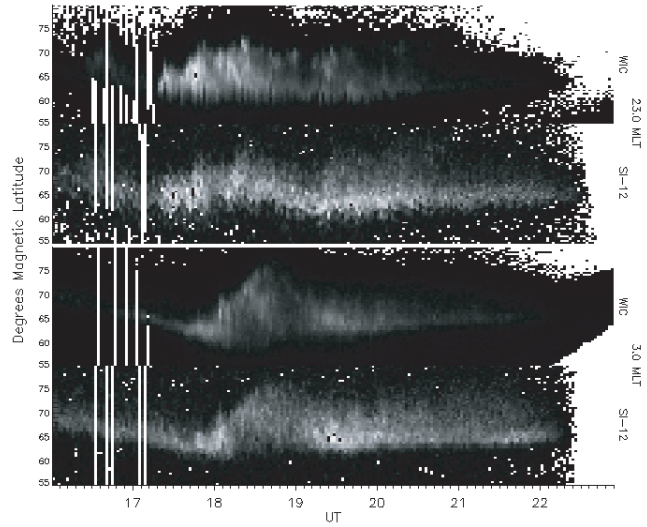


Fig. 2. Keograms for WIC and SI-12 from 16 UT to 23 UT. The top two keograms are taken at 23.0 MLT which is the local time of the pseudo-breakup and close to the first breakup. The bottom two keograms are from 3.0 MLT in order to illustrate the proton aurora later in the sequence of events.

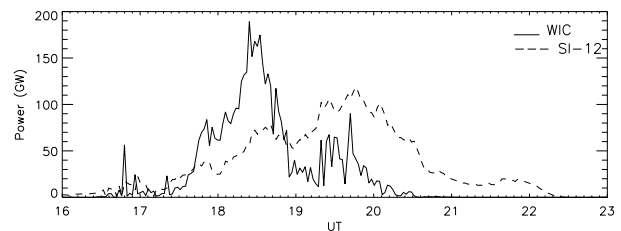


Fig. 3. WIC (LBH) and SI-12 (proton) total auroral substorm power between 16 UT and 23 UT. The solid line is the WIC power and the dashed line is the SI-12 power.

WIC power remains fairly consistent until its rise near 1920 UT. The rise at 1920 UT is also related to secondary electron contamination from the proton precipitation. Figure 4 shows that the ratio of WIC to SI-12 power is near one before 1900 UT. The SI-12 power climbs steadily to nearly five times the WIC power by 1920 UT.

In figure 1, B_z becomes steadily northward at 1940 UT. The recovery phase happens during periods of prolonged northward IMF after a northward turning. Further, examining the keograms in figure 2, it is seen that the WIC camera shows decreasing intensities at both 23.0 MLT and 3.0 MLT. The 23.0 MLT also shows a weak double oval formation. Both of these are characteristics of the recovery phase. Figure 3 also shows decreases in power starting around 1940 UT. This is in agreement as the power is related to the intensity of the auroral oval.

2.1. Pseudo-Breakup - 1720 UT

The pseudo-breakup occurs during the strongly southward IMF and appears to not be IMF triggered. This is being defined as a pseudo-breakup as there is limited poleward and latitudinal expansion.

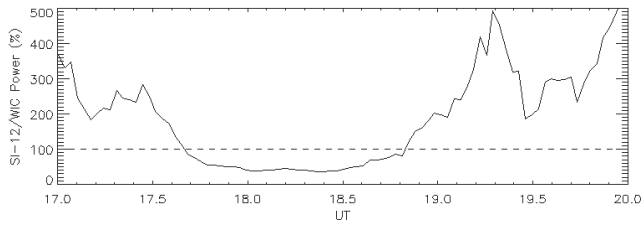


Fig. 4. Power ratio from 17 to 20 UT. The ratio is given as a percentage of power of the SI-12 instrument to the WIC instrument.

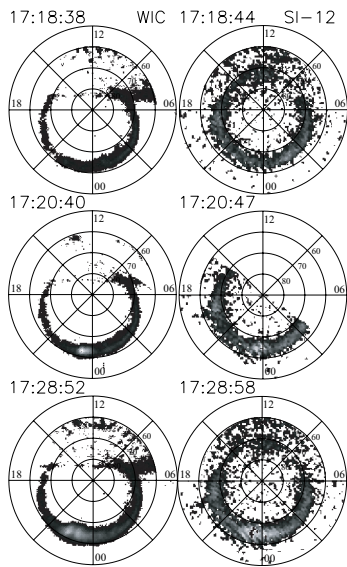


Fig. 5. 1720 UT pseudo-breakup. This is a series of MLT images from the IMAGE WIC and SI-12 cameras. Each row represents one UT time and the left column is WIC and the right column is SI-12.

In figure 5, 1718 UT (the top row) shows the auroral oval to be reasonably quiet. Weak activity does exist and it appears in the same region on both the SI-12 and WIC images. At 1720 UT, a breakup is evident at 23.0 MLT. Both WIC and SI-12 images clearly show a sharp increase in activity. This is confirmed in figure 2 in the 23.0 MLT keograms which also show a sharp boundary in intensity at 1720 UT. Over the next few images (not shown) activity increases and a small auroral bulge forms. At 1728 UT, the pseudo-breakup is already in recovery phase in the WIC image though some activity remains in the SI-12 image. This is confirmed in the 23.0 MLT keograms again as there is a significant decrease in intensity.

2.2. Substorm One - 1737 UT

This substorm occurs during the strongly southward IMF and appears not to be IMF triggered. Although a duskward shift (increase) in B_y occurs at this time and it has been noted that B_y maybe a possible trigger [6]. Solar wind pressure pulses have also been noted to trigger substorms [5] however there is not a complete dataset over that time period in order to determine if the breakup was caused by a change in solar wind dynamic pressure.

At 1735 UT (the top row), in figure 6a, the oval shows weak activity in the WIC image although there is more intense activity in the SI-12 image, mostly in the post-midnight sector. The images at 1737 UT clearly show a breakup at 22.5 MLT in the WIC images and an increase in the intensity of the activity in the pre-midnight sector in the SI-12 image. This means that breakup occurred between 1735 and 1737 as the IMAGE satellite has a two minute cadence. This conclusion is supported by the keograms in figure 2 which also show a significant intensity increase in both the SI-12 and WIC keograms at 23.0 MLT. The keograms at 3.0 MLT also show that the equatorward motion associated with the growth phase has stopped. Figure 3 also clearly shows a dramatic increase in WIC power at this time. The power continues to grow throughout the expansion phase. This is consistent with figure 4 which shows the ratio of SI-12 to WIC power is decreasing throughout the expansion phase.

At 1751 UT, the substorm has reached the beginning of the recovery phase. The oval has begun to decrease latitudinally and in intensity. This intensity decrease can be seen in the keograms at 23.0 MLT. The local maximum power in the SI-12 and WIC occurs at this time. In the final row of images in figure 6a at 1807 UT, the activity has continued to move into the morning sector. Some recovery phase phenomena (double oval formation and increase in the morning sector activity) are visible. The power has decreased from its maximum at 1751 UT for both WIC and SI-12 which is also an indicator of recovery. The WIC power remains larger than the SI-12 power during this period indicating that both WIC and SI-12 power are dropping simultaneously.

2.3. Substorm Two - 1815 UT

This substorm is triggered by a sudden northward turning at 1815 UT following a prolonged (90 minute) strongly southward IMF. Once it peaks, however, the IMF decreases again for 40 minutes down to -10 nT. B_y remains duskward over this time. There is a decrease in the dynamic pressure during the decreasing IMF after onset. As there appears to be no sustained northward IMF, the recovery phase should likely be shortened or non-existent.

In figure 6b, the first row at 1814 UT shows a moderate amount of activity, most of which is still left from the previous substorm seen in figure 6a. There is recovery phenomena seen such as a large latitudinal extent on the morning side, north-south structures, and a double oval. The proton aurora, though not as wide also shows moderate activity in three sectors. Figure 3 shows that there is still significant auroral substorm power.

In the second row, there is obviously a major increase in intensity. The major increase is around 21 MLT with a bifurcation from 21 MLT to 00 MLT as discrete aurora move poleward and the diffuse aurora, still present from the previous substorm moves equatorward during the expansion phase. Proton aurora also brightens, but further east than the WIC image, with the greatest intensity increases near 22.5 MLT. During this time, both WIC and SI-12 power is increasing. The keograms confirm the onset near 1815 UT. The SI-12 keogram at 23.0 MLT is especially good as the SI-12 intensity increases are closest. The 3.0 MLT keograms show tremendous poleward expansion of the oval.

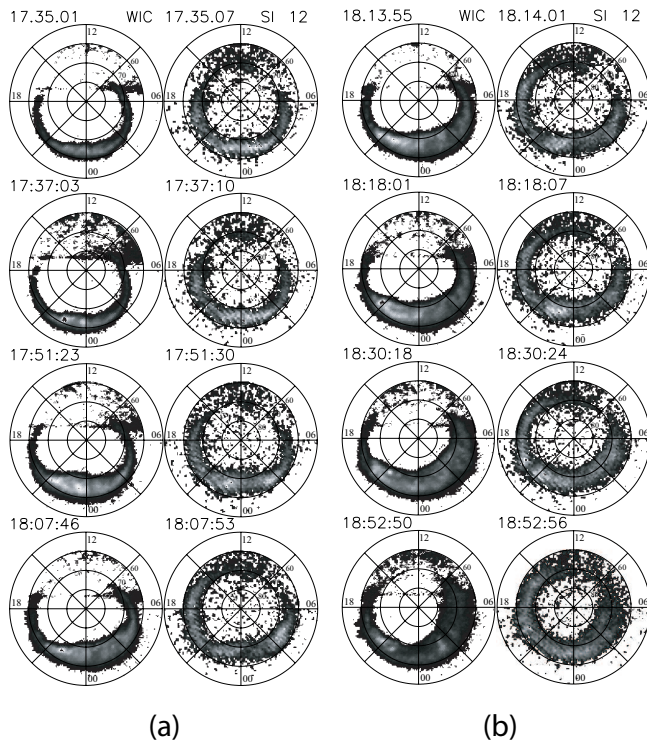


Fig. 6. This is a series of MLT images from the IMAGE WIC and SI-12 cameras. Each row represents one UT time and the left column is WIC and the right column is SI-12. The images in figure (a) represent the first substorm at 1737 UT and figure (b) represents the substorm at 1815 UT.

At 1830 UT, there is a marked decrease in the intensity of the oval as the beginning of the recovery phase of this second substorm starts. A double oval has formed and the morning sector has continued to expand from the recovery phase of the first substorm, now covering over 15° MLAT. Many north-south structures exist from midnight into the morning side as a result of previous recovery phase still continuing. The WIC power curve reaches its maximum at this point, while the SI-12 power curve reaches its maximum a few minutes later. The end of expansion is also evident in the keograms as both the WIC and SI-12 keograms at 23.0 MLT stop poleward motion and the entire oval begins to move equatorward. In the case of the WIC keogram, the intensity also drops off rapidly and a double oval is evident by 1851 UT. The morning side continues to expand latitudinally.

By 1852 UT, the oval appears to be in full recovery phase. The SI-12 image, is also less intense but still has much more activity than the WIC image. This is fully supported by the 23.0 MLT keograms in figure 2. The double oval in the WIC keogram is an indicator of the recovery phase. The WIC power drops off rapidly to a consistent value near 20 GW while the SI-12 power has barely changed at all. Based on the WIC data, the substorm is in full recovery though that is not evident from the SI-12 data. This is clearly shown in figure 4.

2.4. Event - 1900 UT

After the decrease to -10 nT, there is a slow northward turning to 7 nT. At the same time there is an increase in the dynamic

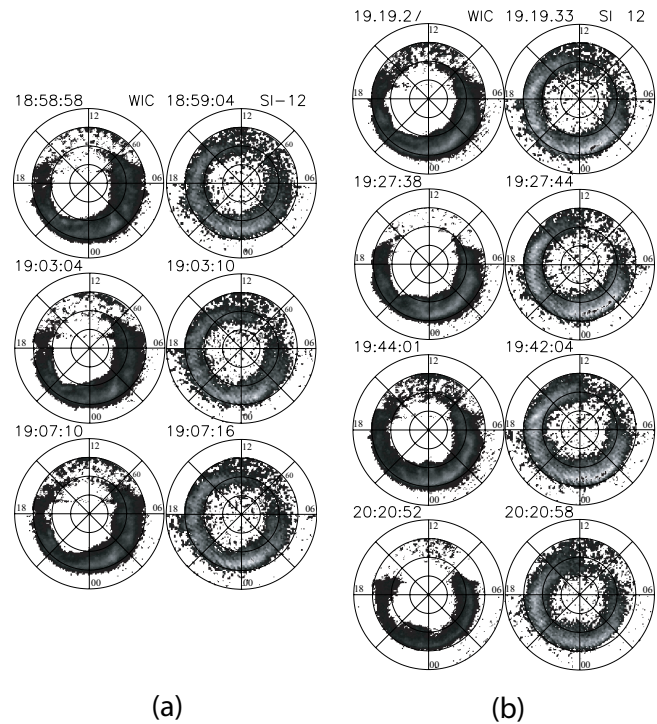


Fig. 7. This is a series of MLT images from the IMAGE WIC and SI-12 cameras. Each row represents one UT time and the left column is WIC and the right column is SI-12. The 1900 UT event is outlined in this set of images. Figures in (a) show the strengthening SI-12 intensities while the WIC intensities remain weak. Figures in (b) show the progression through expansion to recovery 'phases' of the event.

pressure. Based on this solar wind evidence, there is another event, substorm or not, starting at 1900 UT. The SI-12 power also illustrates an event that begins at 1900 UT where as WIC power does not increase until twenty minutes later and never increases above the power of the SI-12.

In figure 7a, at 1859 UT (the first row), the WIC image shows a double oval and weak intensities. The morning sector has expanded over 15° . The SI-12 image, on the other hand, has strong activity near midnight that stretches well into the dusk sector. Four minutes later, the WIC image has continued to decrease in intensity. The SI-12 continues to increase in intensity, expanding further east and latitudinally as if breakup had taken place and the oval was in an expansion phase. Four minutes after that, at 1907 UT, the WIC image continues to show recovery. A slight increase in intensity near 02 MLT is due to proton contamination, secondary electrons are being measured by the WIC imager.

At 1919 UT in figure 7b the SI-12 image intensity has increased dramatically, with a peak near 01 MLT but activity spreading from noon all the way to morning. The WIC image shows activity corresponding to the SI-12 image due to secondary electrons. The SI-12 power locally peaks and stays above 90 GW until 20 UT when it begins to fall off. There are three peaks in the SI-12 power during this time. The WIC power is lower than the SI-12 and is related to secondary electrons. The keograms all show the event happens near 1920 UT based on

intensity increases.

At 1927 UT and 1944 UT the SI-12 images remain active while the WIC images remain weakly active due to secondary electrons. There are north-south features near midnight that are unseen in the SI-12 images. The keograms for these times show the SI-12 is in the expansion phase, the latitudinal expansion still occurring. In the final images, at 2020 UT, the WIC image is nearly retreated into a quiet state. The SI-12 intensity has also decreased significantly. The multi-substorm event is now in full recovery in both WIC and SI-12. The recovery phase started near 1945 UT based on figure 3. The WIC power reaches a quiet state much more quickly than the SI-12 proton power which does not reach a quiet state for about 90 minutes more. This is illustrated in figure 4. After reaching a peak of five times the power, the power ratio drops off as more secondary electrons are measured by the WIC camera. Once the SI-12 power begins to decrease, the secondary electron production decreases rapidly and the WIC power drops to zero. The ratio climbs rapidly during this point and the time is cut off at 20 UT as the ratio becomes infinite shortly thereafter.

3. Discussion and Conclusions

Detailed observations have been presented for a multiple substorm event that clearly show a reduction and depletion of the LBH electron signature after prolonged substorm activity. Several breakups have been presented to occur during this period including both non-IMF and IMF triggered examples. The power measured by the SI-12 and WIC instruments was also presented to illustrate the differences in the observed signals. It is important to note that the calculated power is related to the intensity of the magnetic local time images.

The event occurring at 1900 UT onwards is a strong proton event fitting the the substorm description of growth, onset, expansion and recovery phases. The lack of a primary electron signature in the LBH band is interesting. However, the precipitating protons evoke a secondary electron response in the LBH range measured by WIC. Figures 3 and 4 clearly illustrate this point.

In figure 3, the SI-12 power is smaller than the WIC power starting after the onset of the first substorm. This is also clear in figure 4. The LBH signal is strong until also 1900 UT while in the recovery phase of the second substorm. During the recovery phase, the proton signature measured by SI-12 remains high and becomes greater than the WIC power near 1852 UT. The WIC camera continues to display recovery phase characteristics event as the protons bring to enter into another active cycle. Figure 3 shows that the power of the SI-12 is higher than WIC power. The WIC power displayed is contaminated by secondary electrons elevating the power artificially. Once the power calculated from SI-12 observations begins to decrease (beginnings of the recovery phase), the WIC power drops extremely rapidly as the secondary electron contamination is removed. Figure 4 shows the ratio getting closer to one until such time as the recovery phase begins and the ratio increases rapidly. As the WIC power reaches zero the power calculated from SI-12 remains above zero for two more hours. This leaves us with the question: Is this proton event actually a substorm with a depleted electron signature?

Several possible explanations may account for some or all of the depletion of the electrons in the LBH. Perhaps the plasma source region has been reduced in electrons of the proper energies to produce an LBH signal. Since the bounce period for electrons is 1000 times shorter, the electrons deplete faster. This sets up a parallel electric current due to charge separation. It may be possible to measure this current during this time and observe the magnitude of the current. This would provide insight into the behaviour of the electrons in the source region. Mapping the footprint back into the tail and examining where the source region is and potentially what L-shell it is on during the entire multiple-substorm event could provide insight on the type of source region involved.

Based on the ACE data and the keograms, it could be that the electron loss cone may not have a chance to completely refill between substorms leaving a fuller proton loss cone later in the event. Considering B_z , if the electron loss cone starts to fill, at 1642 UT, the first optical signature of precipitation starts at 1720 UT with the pseudo break and then the non-IMF triggered substorm. During this time, the magnetosphere should continue to be loaded. At 1815 UT, the second substorm occurs. After onset, it appears to continue to load based on B_z . However, if the precipitation has emptied the loss cone significantly by this point, the short time period between the second substorm and the final event may not allow enough loading before B_z remains northward.

The energy of particle precipitation is dissipated in several ways including heat and light. Due to the prolonged precipitation, the atmosphere is being heated. This heating causes the scale height of the atmosphere to increase. Since electrons penetrate deeper into the atmosphere than protons due to their smaller collision frequency. O_2 is a major absorber in the LBH range, therefore with the increase of O_2 at higher altitudes more of the LBH photons are absorbed.

What has been useful in this event is the determination of the beginning of the recovery phase based the power of IMAGE-FUV. Pulkkinen's paper [10] used the AE to determine the possible start of the recovery phase. While the AE is taken at a higher frequency than the IMAGE data, due to lack of magnetometers the AE can no longer be calculated with accuracy. The use of auroral substorm or hemispheric power of the global images may provide a very good indicator of the start of the recovery phase.

Future work may include looking for other examples of prolonged events where the proton power calculated from the SI-12 is greater than the WIC power. If several more of these events can be identified, what ramifications does this have on interpreting substorms? Identification of other data sets that may maybe used in defining ionospheric and auroral behaviour will be important. FAST and DMSP may provide particle measurements in the near Earth environment. Also, gathering data from downtail sources such as Geotail and Cluster may give hints to the magnetospheric topology that leads to such optical auroral observations as this.

4. Acknowledgements

The authors would like to thank Benoit Hubert for valuable discussions and James Weygand for the Weimer-mapped ACE

data. This research is supported by a grant from the Natural Science and Engineering Research Council of Canada.

References

1. Carbary, J. F., Liou, K., Lui, A. T. Y., Newell, P. T. and C.-I. Meng, Blob analysis of auroral substorm dynamics, *Journal of Geophysical Research*, *105*, 16083–16091, 2000.
2. Frey, H. U., Mende, S. B., Immel, T. I., Gerard, J.-C., Hubert, B., Habraken, S., Spann, J., Gladstone, G. R., Bisikalo, D. V., and Shematovich, V. I., Summary of Quantitative Interpretation of IMAGE Far Ultraviolet Auroral Data, *Space Science Reviews*, *109*, 255–283, 2003.
3. Hubert, B., Gerard, J.-C., Bisikalo, D. V., Shematovich, V. I., and Soloman, S. C., The role of proton precipitation in the excitation of the auroral FUV emissions, *Journal of Geophysical Research*, *106*, 15.1–15.1221475–21494, 2001 2002.
4. Hubert, B., Gerard, J.-C., Evans, D. S., Meurant, M., Mende, S. B., Frey, H. U., Immel, T. J., Total electron and proton energy input during auroral substorms: remote sensing with IMAGE-FUV, *Journal of Geophysical Research*, *107*, 15.1–15.12, 2002.
5. Lyons, L. R., A new theory for magnetic substorms, *Journal of Geophysical Research*, *100*, 19069–19081, 1995.
6. Lyons, L. R., Blanchard, G. T., Samson, J. C., R. P. Lepping, T. Yamamoto, and T. Moretto, Coordinated observations demonstrating external substorm triggering, *Journal of Geophysical Research*, *102*, 27039–27051, 1997.
7. Mende, S. B. et al., Far ultraviolet imaging from the IMAGE spacecraft: 2. Wideband Imaging Camera, *Space Science Reviews*, *91*, 271–286, 2000.
8. Mende, S. B. et al., Far ultraviolet imaging from the IMAGE spacecraft: 3. Spectral Imaging of Lyman-alpha and OI 135.6 nm, *Space Science Reviews*, *91*, 287–318, 2000.
9. Mende, S. B., Frey, H. U., Immel, T. J., Gerard, J.-C., Hubert, B., Fuselier, S. A., Global Imaging of Proton and Electron Aurorae in the Far Ultraviolet, *Space Science Reviews*, *109*, 211–254, 2003.
10. Pulkkinen, T. I., Baker, D. N., Toivanen, P. K., Pellinen, R. J., Friedel, R. H. W., and Korth, A., Magnetospheric field and current distributions during the substorm recovery phase, *Journal of Geophysical Research*, *99*, 10955–10966, 1994.